

Turbulence structure in a boundary layer with two-dimensional roughness

R. J. VOLINO¹†, M. P. SCHULTZ² AND K. A. FLACK¹

¹Mechanical Engineering Department, United States Naval Academy, Annapolis, MD 21402, USA

²Naval Architecture and Ocean Engineering Department, United States Naval Academy, Annapolis, MD 21402, USA

(Received 18 August 2008; revised 9 April 2009; accepted 10 April 2009)

Turbulence measurements for a zero pressure gradient boundary layer over a two-dimensional roughness are presented and compared to previous results for a smooth wall and a three-dimensional roughness (Volino, Schultz & Flack, *J. Fluid Mech.*, vol. 592, 2007, p. 263). The present experiments were made on transverse square bars in the fully rough flow regime. The turbulence structure was documented through the fluctuating velocity components, two-point correlations of the fluctuating velocity and swirl strength and linear stochastic estimation conditioned on the swirl and Reynolds shear stress. The two-dimensional bars lead to significant changes in the turbulence in the outer flow. Reynolds stresses, particularly $\overline{v'^2}^+$ and $-\overline{u'v'}^+$, increase, although the mean flow is not as significantly affected. Large-scale turbulent motions originating at the wall lead to increased spatial scales in the outer flow. The dominant feature of the outer flow, however, remains hairpin vortex packets which have similar inclination angles for all wall conditions. The differences between boundary layers over two-dimensional and three-dimensional roughness are attributable to the scales of the motion induced by each type of roughness. This study has shown three-dimensional roughness produces turbulence scales of the order of the roughness height k while the motions generated by two-dimensional roughness may be much larger due to the width of the roughness elements. It is also noted that there are fundamental differences in the response of internal and external flows to strong wall perturbations, with internal flows being less sensitive to roughness effects.

1. Introduction

The importance of surface roughness is well known for wall-bounded flows. The fluid must move around and over the roughness elements, so the near-wall flow structure is clearly altered. Roughness typically increases drag in turbulent boundary layers due to pressure forces on the roughness elements. The near-wall streaks documented by Kline *et al.* (1967) in smooth-wall boundary layers typically have a spacing of about 100 wall units, and are undoubtedly disrupted by roughness elements of this size or larger. While the flow structure near the roughness elements must be affected, Jiménez (2004) notes that as long as the roughness height k is not too large relative to the boundary layer thickness δ most of the evidence in the literature shows outer layer similarity between rough and smooth wall boundary

† Email address for correspondence: volino@usna.edu

layers. Roughness will alter the wall shear and the growth of the boundary layer, but when the outer flow is normalized using the friction velocity u_τ and δ similarity is observed. This similarity was said to hold as long as $k/\delta < 1/50$. This is consistent with Townsend's (1976) Reynolds number similarity hypothesis. Schultz & Flack (2007) critically tested this hypothesis for the conditions proposed by Townsend ($k \ll \delta$ and high Reynolds numbers), experimentally studying the boundary layer over a sanded surface. They considered cases ranging from the hydrodynamically smooth to the fully rough regimes and found excellent agreement in the Reynolds stresses and velocity triple products outside the near-wall region. Other studies since the Jiménez (2004) review include Flack, Schultz & Shapiro (2005), Kunkel & Marusic (2006) and Wu & Christensen (2007). All found outer layer similarity for boundary layers over various rough surfaces. Large roughness elements have also been tested. Castro (2007) conducted experiments with very large three-dimensional roughness (mesh, staggered cubes, gravel chips) and found that mean flow similarity held for $k/\delta < 1/10$. Flack, Schultz & Connelly (2007) observed outer layer similarity in turbulence quantities. They conducted experiments with three-dimensional mesh and sandpaper surfaces with a large range of roughness heights. They observed that roughness effects were confined to a roughness sublayer within $5k$ or $3k_s$ of the surface, where k_s is the equivalent sandgrain height. No critical value of k/δ was observed for breakdown of similarity. Effects of roughness were seen farther from the wall as $5k$ or $3k_s$ became a larger fraction of δ .

Similarity in turbulence structure was reported by Volino, Schultz & Flack (2007) who experimentally studied boundary layers over a smooth wall and a wall covered with three-dimensional mesh. The turbulence structure was quantified through turbulence spectra, the probability density function of the swirl strength, two-point spatial correlations of turbulence quantities and swirl, structure angles and length scales of correlations. The dominant structure in both the rough-wall and smooth-wall outer layers was the vortex packet. Wu & Christensen (2007) reported similarity in the outer layer turbulence structure for flows over smooth walls and walls with replicated turbine blade roughness. The similarity observed in boundary layers has also been found in channel flows. Flores & Jiménez (2006), for example, conducted a direct numerical simulation (DNS) study of a symmetric channel flow with three-dimensional disturbances on both bounding walls. The effect of the disturbances was confined to a layer near the wall. The structure and dynamics of the turbulence in the outer flow was virtually unchanged by the nature of the wall.

The studies noted above all considered three-dimensional k -type roughness. The consensus of most studies is that outer layer similarity with smooth-wall boundary layers holds for a large range of three-dimensional roughness types and sizes. Two-dimensional k -type roughness may, however, cause different behaviour. Two-dimensional transverse rods were studied by Krogstad & Antonia (1999). They reported an increase in the Reynolds stresses in the outer layer in comparison to smooth-wall results. The Reynolds stress profile shapes were significantly altered over the two-dimensional rods. The streamwise rod spacing, p , in this case was four times the rod diameter. Keirsbulck *et al.* (2002) reported results for boundary layer experiments with two-dimensional transverse bars and $p/k = 3.33$. They found reasonable similarity with smooth-wall flows for the Reynolds stresses in the outer flow. Djenidi *et al.* (2008) conducted experiments with two-dimensional transverse square bars and p/k ranging from 8 to 16. They noted differences in the turbulence structure and larger Reynolds stresses in the outer layer than for smooth-wall cases. Results varied with bar spacing, with the strongest effect at larger spacing. This

variation may explain the lesser effect of roughness observed by Keirsbulck *et al.* (2002), who used a smaller spacing. Lee & Sung (2007) conducted a DNS for a turbulent boundary layer over a wall with two-dimensional disturbances. The disturbances modelled two-dimensional transverse square bars with $p/k=8$. Lee & Sung (2007) reported an increase of all the Reynolds normal stresses and the Reynolds shear stress across most of the boundary layer. Velocity triple products in the outer layer, particularly the vertical transport of the Reynolds shear stress, were also affected by the roughness.

In turbulent channel flows, two-dimensional roughness does not appear to produce the differences observed in boundary layers. Krogstad *et al.* (2005) conducted experiments and DNS for symmetric channel flow with two-dimensional k -type transverse square bars and $p/k=8$ on both bounding walls. Differences from the smooth-wall case were not observed in the outer flow. Effects on the Reynolds stresses were confined to within $5k$ of the wall. Burattini *et al.* (2008) conducted experiments and DNS for an asymmetric channel with two-dimensional transverse square bars on only one wall. The bar spacing was $p/k=4$. The turbulence structure was similar to that on a smooth wall, with the exception of differences in the streamwise component of the turbulence near the rough wall. Ikeda & Durbin (2007) conducted DNS and RANS simulations for asymmetric channels with two-dimensional square transverse bars spaced at $p/k=10$. Their focus was mainly on the near-wall region, where they observed significant differences in the near-wall structure between smooth and rough cases. They noted differences between their results and the expected results for a symmetric channel, which may help explain differences observed in other asymmetric channel studies. They also noted the limitations of RANS calculations with rough-wall flows.

The present study addresses two general questions raised by the above discussion. First, do two-dimensional and three-dimensional roughness affect turbulent boundary layers differently? The existing evidence suggests that the answer is yes, which raises the questions of why and how they differ. Second, do the outer layers of turbulent boundary layers and turbulent channel flows react differently in response to surface roughness and why? These questions are addressed through documentation of turbulence statistics, swirl and spatial correlations in turbulent boundary layers over walls with two-dimensional and three-dimensional roughness.

2. Experiments and data processing

Experiments were conducted in the water tunnel described by Volino *et al.* (2007). The test section was 2 m long, 0.2 m wide and nominally 0.1 m tall. The lower wall was a flat plate which served as the test wall. The upper wall was adjustable and set for a zero streamwise pressure gradient with the free stream velocity set to 0.5 m s^{-1} . Although the boundary layer was as thick as 54 mm on the rough test wall, the displacement of the upper wall required to maintain a zero pressure gradient (30 mm) and the thin boundary layer on the smooth upper wall resulted in a free stream between the upper and lower boundary layers that was at least 50 mm thick. The acceleration parameter, defined as

$$K = \frac{\nu}{U_e^2} \frac{dU_e}{dx} \quad (2.1)$$

was less than 5×10^{-9} . The upper wall and sidewalls provided optical access. The test wall was an acrylic plate machined with two-dimensional transverse square bars, as

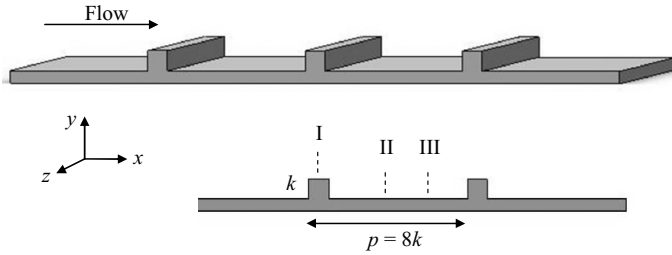


FIGURE 1. Schematic illustration of two-dimensional bar roughness.

shown in figure 1. The bar height was $k = 1.7$ mm. The bar spacing was $p/k = 8$. This geometry is expected to behave as k -type roughness according to Perry, Schofield & Joubert (1969) in which the downward shift in the log law, ΔU^+ , scales on the roughness Reynolds number k^+ . The roughness geometry is identical to that used in the DNS boundary layer study of Lee & Sung (2007) and the channel flow study of Krogstad *et al.* (2005). The wall was painted black to facilitate optical measurements. The boundary layer was tripped near the leading edge with a 0.8 mm diameter wire, ensuring a turbulent boundary layer. Smooth and three-dimensional rough wall comparison cases were documented in Volino *et al.* (2007). An acrylic test plate was used for the smooth-wall case. A woven wire mesh was affixed to a similar plate for the three-dimensional rough-wall case. The mesh spacing was $t = 1.69$ mm, and the mesh wire diameter was 0.26 mm, resulting in a peak to trough roughness height of $k = 0.52$ mm. The height of the mesh roughness is considerably smaller than the present bar height. Flack *et al.* (2007) studied the flow over sandgrain and mesh roughness for a wide range of roughness sizes, and observed similarity with smooth-wall results in all cases. Included were cases with the ratio of the roughness height to boundary layer thickness smaller than the mesh of Volino *et al.* (2007) and cases with this ratio larger than that of the bars in the present study. The difference in roughness height between the mesh and the bars is not, therefore, expected to affect the results. Mesh and sandgrain roughness produced similar results in Flack *et al.* (2007), suggesting that the shape of the three-dimensional roughness elements also does not play a significant role. To further investigate the role of roughness size and shape, a comparison case is taken from Cheng & Castro (2002) with three-dimensional cube roughness.

Flow was supplied to the test section from a 4000 L cylindrical tank. Water was drawn from the tank to two variable speed pumps operating in parallel and then sent to a flow conditioning section consisting of a diffuser containing perforated plates, a honeycomb, three screens and a three-dimensional contraction. The test section followed the contraction. The free stream turbulence level was less than 0.5%. Water exited the test section through a perforated plate emptying into the cylindrical tank. The test fluid was filtered and deaerated water. A chiller was used to keep the water temperature constant to within 1°C during all tests.

Boundary layer velocity measurements were obtained with a TSI FSA3500 two-component laser Doppler Velocimeter (LDV). The LDV consists of a four-beam fibre optic probe that collects data in backscatter mode. A custom-designed beam displacer was added to the probe to shift one of the four beams, resulting in three co-planar beams that can be aligned parallel to the wall. Additionally, a 2.6:1 beam expander was located at the exit of the probe to reduce the size of the measurement volume. The resulting probe volume diameter (d) was 45 μm with a probe volume length (l)

of $340\ \mu\text{m}$. The corresponding measurement volume diameter and length in viscous length scales were $d^+ = 1.5$ and $l^+ = 11.6$.

Measurements were made 1.0m downstream of the trip, where the turbulent Reynolds number matched the value of the smooth-wall comparison case. For the velocity profile, the LDV probe was traversed to approximately 40 locations within the boundary layer with a Velmex three-axis traverse unit. The virtual origin for the velocity profiles was 1.6mm below the top of the bars. The traverse allowed the position of the probe to be maintained to $\pm 5\ \mu\text{m}$ in all directions. A total of 50 000 random velocity samples were obtained at each location in the boundary layer. The data were collected in coincidence mode. The flow was seeded with $3\ \mu\text{m}$ diameter alumina particles. The seed volume was controlled to achieve acceptable data rates while maintaining a low burst density signal (Adrian 1983). Measurements were made at three streamwise stations over one roughness bar spacing as shown in figure 1. Station I was located at the centre of a roughness element, station II was located $3k$ downstream of station I, and station III was located $5.75k$ downstream of station I. These are the same locations used by Lee & Sung (2007).

Flowfield measurements were acquired using particle image velocimetry (PIV). A streamwise-wall normal (xy) plane was acquired at the spanwise centreline of the test section. Streamwise-spanwise (xz) planes were acquired at $y/\delta = 0.1$ and 0.4 . The flow was seeded with $3\ \mu\text{m}$ diameter alumina particles. The light source was a Nd:YAG laser set for an $850\ \mu\text{s}$ interval between pulses for each image pair. The field of view in the xy -plane was $135\text{ mm} \times 100\text{ mm}$, extending from near the wall into the free stream. In the xz -plane the field of view was $112\text{ mm} \times 84\text{ mm}$, centred about the midspan of the test section. A CCD camera with a 1376×1024 pixel array was used. Image processing was done with TSI Insight 3G software. Velocity vectors were obtained using 16 pixel square windows with 50% overlap. For each measurement plane, 2000 image pairs were acquired for processing. For consistency in comparison, the raw image pairs acquired by Volino *et al.* (2007), which had originally been processed with TSI Insight 6.0 software, were reprocessed with the Insight 3G software. Changes in the results due to the reprocessing were not significant.

The data processing techniques used to compute the mean velocity, turbulence statistics and wall shear are described in detail in Schultz & Flack (2007). The techniques used to compute spatial correlations and swirl strength are described in Volino *et al.* (2007) and defined again below.

Two-point spatial correlations were done for each measurement plane. In the xy -plane the correlation is defined at the wall normal position y_{ref} as

$$R_{AB}(y_{ref}) = \frac{\overline{A(x, y_{ref})B(x + \Delta x, y_{ref} + \Delta y)}}{\sigma_A(y_{ref})\sigma_B(y_{ref} + \Delta y)}, \quad (2.2)$$

where A and B are the quantities of interest at two locations separated in the streamwise and wall normal directions by Δx and Δy , and σ_A and σ_B are the standard deviations of A and B at y_{ref} and $y_{ref} + \Delta y$, respectively. At every y_{ref} , the overbar indicates the correlations were averaged among location pairs with the same Δx and Δy , and then time averaged over the 2000 vector fields. Correlations of u , v , the swirl strength and all cross-correlations were considered.

For the xz -planes, the correlation is defined as

$$R_{AB} = \frac{\overline{A(x, z)B(x + \Delta x, z + \Delta z)}}{\sigma_A\sigma_B}, \quad (2.3)$$

where A and B are the quantities of interest at two locations separated in the streamwise and spanwise directions by Δx and Δz , and σ_A and σ_B are the standard deviations of A and B based on data in the full plane for the 2000 vector fields. The correlations were averaged among all locations with the same Δx and Δz , and then time averaged. The same averaging techniques were used by Tomkins & Adrian (2003) and Ganapathisubramani *et al.* (2005).

The swirl strength λ can be used to locate vortices. It is closely related to the vorticity, but discriminates between vorticity due only to shear and vorticity resulting from rotation. It is defined as the imaginary part of the complex eigenvalue of the local velocity gradient tensor, and is defined as follows (Zhou *et al.* 1999):

$$[\mathbf{d}_{ij}] = [v_r \ v_{cr} \ v_{ci}] \begin{bmatrix} \lambda_r & & \\ & \lambda_{cr} \ \lambda_{ci} & \\ & -\lambda_{ci} \ \lambda_{cr} & \end{bmatrix} [v_r \ v_{cr} \ v_{ci}]^{-1}, \quad (2.4)$$

where $[\mathbf{d}_{ij}]$ is the velocity gradient tensor. It is used in the present study in a two-dimensional form as explained in several studies including Hutchins, Hambleton & Marusic (2005). A more complete discussion is available in Chong, Perry & Cantwell (1990). By definition, λ is always ≥ 0 , but a sign can be assigned based on the local vorticity to show the direction of rotation. Swirl strength λ is assumed signed in the present work. In the xy -plane, λ can be used to identify the heads of hairpin vortices, and in the xz -plane λ can identify the legs of these vortices.

Linear stochastic estimation (LSE) was used to estimate the average velocity field associated with specific conditioning events in the flow. The application of the technique is similar to that used by Hambleton, Hutchins & Marusic (2006) and Christensen & Adrian (2001). A complete derivation is available in Adrian & Moin (1988). The LSE in the xy -plane was computed as

$$\begin{aligned} \langle u'_j(x + \Delta x, y_{ref} + \Delta y) | B(x, y_{ref}) \rangle \\ = \frac{\langle B(x, y_{ref}) u'_j(x + \Delta x, y_{ref} + \Delta y) \rangle}{\langle B(x, y_{ref}) B(x, y_{ref}) \rangle} B(x, y_{ref}), \end{aligned} \quad (2.5)$$

where u'_j is the fluctuating velocity vector at the distances Δx and Δy from the conditioning event B . At a given y_{ref} , averaging was done among location pairs with the same Δx and Δy , and then over the 2000 vector fields. The result is the average velocity vector field associated with the conditioning event. Several conditioning events were considered, and results for two that were found most useful are presented below. Prograde swirl ($B = \lambda_p$), as used by Hambleton *et al.* (2006) and Christensen & Adrian (2001), was useful for identifying the velocity field associated with a hairpin vortex head at the reference location. The term prograde, as used by Wu & Christensen (2006), refers to vortices rotating in the direction exhibited by the hairpin heads, as induced by the mean shear. Vortices rotating in the opposite direction are termed retrograde. The other conditioning event for LSE was $u'v' < 0$ ($B = u'v'_n$). This criteria uses the combination of quadrants Q2 (ejections) and Q4 (sweeps) to determine the average vector field associated with events contributing towards the mean Reynolds shear stress.

3. Results

The boundary layer thickness, friction velocity and other quantities from the velocity profile of the present case and the comparison cases are presented in table 1. The

Wall	x (m)	U_e (m s ⁻¹)	δ (mm)	u_τ (m s ⁻¹)	Re_θ $= U_e \theta / \nu$	$Re_\tau = \delta^+$ $= u_\tau \delta / \nu$	k_s^+ $= k_s u_\tau / \nu$	k/δ
Smooth	1.50	1.255	35.2	0.0465	6069	1772		
Three-dimensional rough (mesh)	1.08	1.247	36.8	0.0603	7663	2438	112	0.014
Two-dimensional rough (bars)	1.00	0.50	54.6	0.0341	4260	1790	755	0.031

TABLE 1. Boundary layer parameters.

results presented were taken at station II (figure 1). No significant variation was observed in the results from the three stations except for a region within about $3k$ of the wall. For the rough-wall cases, the skin friction coefficient was found to be invariant with Reynolds number, indicating fully rough conditions. This is consistent with the roughness Reynolds numbers based on the equivalent sand roughness height, $k_s^+ = k_s u_\tau / \nu$, which are 112 (three-dimensional) and 755 (two-dimensional). The roughness Reynolds number is given by the following (Schlichting 1979):

$$\Delta U^+ = \frac{1}{\kappa} \ln k_s^+ - 3.5, \quad (3.1)$$

where ΔU^+ is the roughness function. The friction velocity u_τ was determined using the Clauser chart method with $\kappa = 0.41$ and $B = 5.0$. The uncertainty in u_τ was $\pm 3\%$ and $\pm 6\%$ for the smooth- and rough-wall cases, respectively. The total stress method was also used to evaluate u_τ , and the resulting values agreed with those from the Clauser chart method to within 2%. Details of both methods are given in Flack *et al.* (2005). The uncertainties in the boundary layer thickness (based here on $U/U_e = 0.99$) and momentum thickness were 7% and 4%, respectively.

3.1. Mean velocity and turbulence profiles

Before acquisition of data at the condition shown in table 1, a velocity profile was acquired with the facility set for a free stream velocity corresponding to $Re_\tau = 520$. This allowed a comparison to the DNS of Lee & Sung (2007), who considered two-dimensional bars of the same size and spacing at $Re_\tau = 550$. The mean velocity profile in defect coordinates and the Reynolds stresses in inner scaling are shown in figure 2. The mean velocity and $\overline{u'^2}^+$ profiles of the experiment and DNS agree well at all locations. Some differences are visible in $\overline{v'^2}^+$ and $-\overline{u'v'}^+$ for $y^+ < 50$, but agreement in the outer layer is very good for these quantities as well. Lee & Sung (2007) noted higher Reynolds stresses in the outer region than for a smooth wall boundary layer, and the present results agree.

Mean velocity profiles for the cases in table 1 are shown in figure 3 in both inner and defect coordinates. The inner normalized coordinates show a much larger shift for the two-dimensional roughness. No clear differences are visible in defect coordinates. Similarity in the mean profiles was also noted by Krogstad & Antonia (1999) for two-dimensional and three-dimensional roughness. These results indicate that the mean flow in the outer layer is fairly insensitive to surface conditions.

The Reynolds stresses for the two-dimensional and three-dimensional roughness cases in outer coordinates are compared to the smooth-wall results in figures 4–6. Also shown are the two-dimensional roughness results of Krogstad & Antonia (1999), who used rods spaced at $p/k = 4$, and the three-dimensional roughness

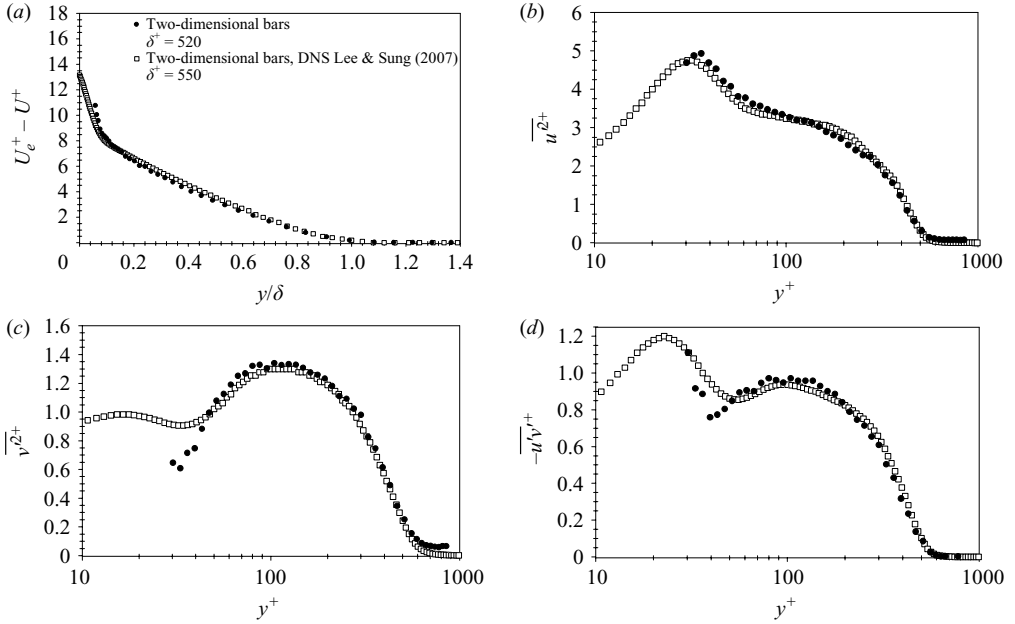


FIGURE 2. Low Reynolds number ($Re_\tau = 520$) comparison of present experiments to DNS of Lee & Sung (2007), (a) mean velocity, (b) streamwise Reynolds normal stress, (c) wall-normal Reynolds stress and (d) Reynolds shear stress.

results of Cheng & Castro (2002), who used staggered rows of cubes spaced at $p/k=2$ in both the streamwise and spanwise directions. The cubes resulted in $Re_\theta = 10473$, $Re_\tau = 4670$, $k/\delta = 0.083$ and $k_s/k = 1.90$. For all the Reynolds stresses, the smooth and three-dimensional mesh cases agree, as previously shown in Volino *et al.* (2007). The results with the three-dimensional cubes also agree reasonably well. Some differences are visible very near the wall, which is expected since different types of roughness can affect the roughness sublayer differently. Differences near the edge of the boundary layer may result from different free stream turbulence levels or the higher Reynolds numbers in the case with cubes. The $\overline{u'^2}^+$ normal stress is shown in figure 4. The present two-dimensional roughness values in the outer layer are somewhat higher than in the comparison cases, but the differences are not large. The $\overline{v'^2}^+$ normal stress is shown in figure 5. The two-dimensional roughness results of the present study and Krogstad & Antonia (1999) agree, and are roughly 20% higher than those in the three-dimensional rough- and smooth-wall cases. The difference extends well into the outer region to y/δ of about 0.7. Similar differences are present in the Reynolds shear stress, shown in figure 6. Differences in $\overline{v'^2}^+$ and $-\overline{u'v'}^+$ were also noted in the outer layer by Lee & Sung (2007), however they also noted similar increases in $\overline{u'^2}^+$. The differences which are present between the three-dimensional cube and three-dimensional mesh cases are opposite in sign to the differences between the three-dimensional mesh and two-dimensional bar cases. Since the two-dimensional bar height is between the cube and mesh heights in terms of k/δ , and the cubes have the same square-edged shape as the bars, the differences between the two-dimensional and three-dimensional cases are not due to the size or square-edged nature of the roughness. The differences must be due to the change from two to three-dimensional elements.

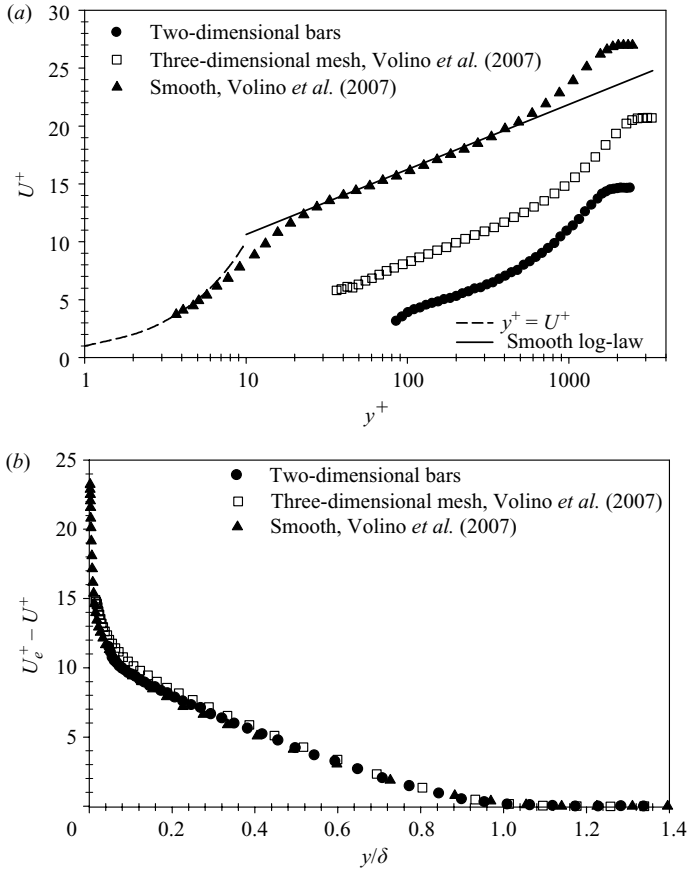


FIGURE 3. Mean velocity profiles in (a) inner variables and (b) velocity defect form.

The present results along with the body of literature show that two-dimensional roughness affects the boundary layer differently than three-dimensional roughness. As noted above, Flack *et al.* (2007) found that for three-dimensional roughness, the roughness sublayer was confined to within about $5k$ or $3k_s$ of the wall. For the three-dimensional cases noted above, $5k$ and $3k_s$ are within a factor of 2 of each other, and similarity with the smooth wall case is observed in the outer layer. For the two-dimensional case, however, $3k_s$ is 8 times larger than $5k$. If the roughness sublayer is taken as $5k$, outer layer similarity with the smooth-wall case is disrupted. If $3k_s$ is used as the criteria, then the two-dimensional bars cause the roughness sublayer to extend to the edge of the boundary layer, thereby eliminating the outer layer. This is considered further in §4. Whether by changing the outer layer or extending the roughness sublayer, the two-dimensional bars must affect the turbulence structure far from the wall. The structure is considered next.

3.2. Velocity fields: xy -plane

Typical instantaneous velocity vector fields in the streamwise-wall normal plane are shown in figure 7 for the two-dimensional and three-dimensional rough-wall cases. A Galilean decomposition has been applied, with the uniform convection velocity $0.7U_e$ subtracted from each field. The hairpin vortices in a packet become visible if their common convection velocity is subtracted from the instantaneous field. Hairpin heads

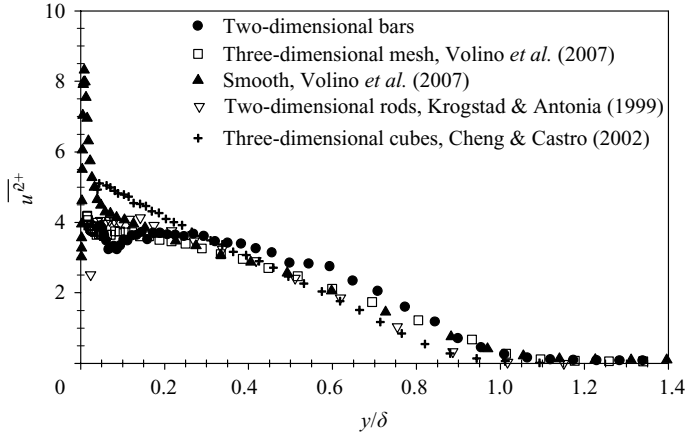


FIGURE 4. Streamwise Reynolds normal stress profiles.

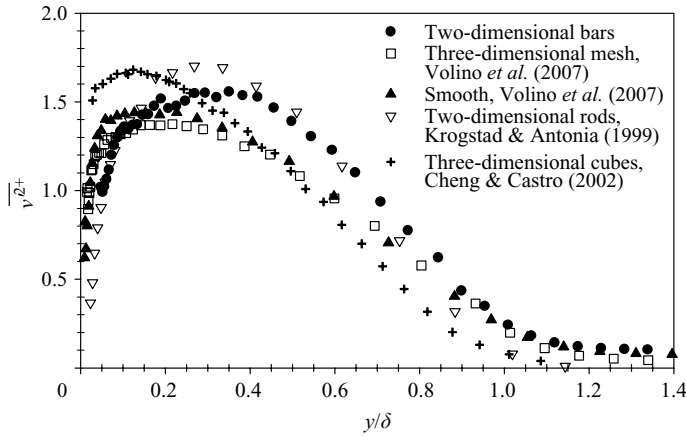


FIGURE 5. Wall-normal Reynolds normal stress profiles.

exhibit prograde rotation, which is clockwise in figure 7. Superimposed on the vectors in figure 7 are contours of signed swirl strength. Hairpin packets typically appear as a line of vortices, inclined at about 10° – 15° to the wall. In the three-dimensional rough-wall case (figure 7a) a field has been chosen which shows the end of a mature hairpin packet on the left ($x/\delta < 0.6$) with another hairpin packet extending nearly the entire width of the image ($0 < x/\delta < 1.9$). Such packets did not appear in every instantaneous field, but they were very common for both the three-dimensional rough- and smooth-wall cases, as shown in Volino *et al.* (2007). Similar packets were also observed in the two-dimensional rough-wall case, but they were also accompanied by larger scale events, as shown in figure 7(b). Figure 7(b) shows large-scale eruptions of fluid extending to the edge of the boundary layer. Events extending this far into the outer part of the boundary layer were very rare in the smooth- and three-dimensional rough-wall cases, but they were fairly common in the two-dimensional rough-wall case, appearing in roughly 10% of the instantaneous velocity fields.

The large-scale events are believed to originate on the wall at the bars. In the various studies listed above with close-packed three-dimensional roughness, large contiguous open spaces between the roughness elements were not present, so recovery

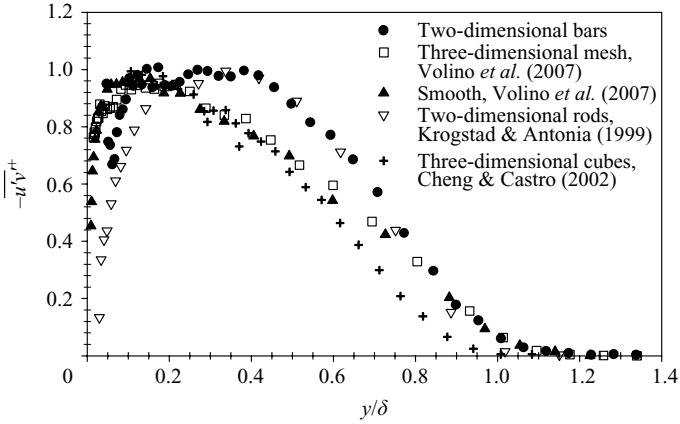


FIGURE 6. Reynolds shear stress profiles.

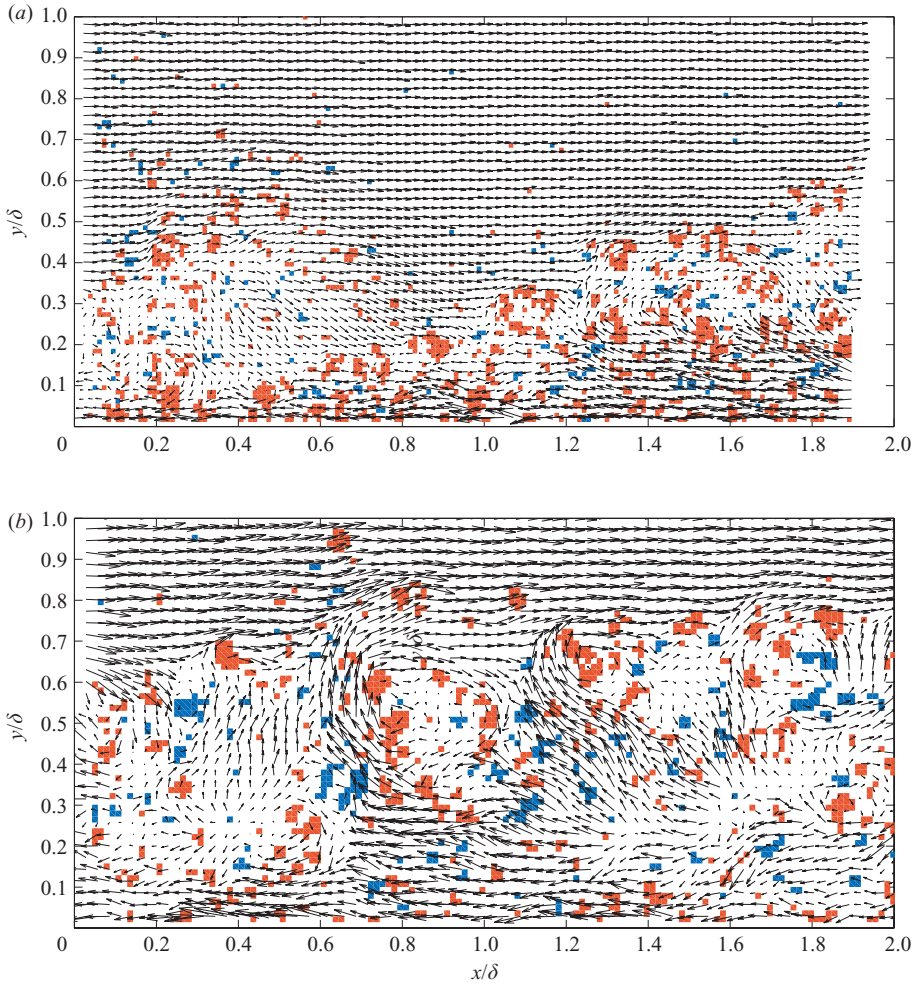


FIGURE 7. Typical instantaneous velocity field in xy -plane with prograde swirl (red shading) and retrograde swirl (blue shading) superimposed, (a) three-dimensional rough wall and (b) two-dimensional rough wall.

of the instantaneous velocity profile in the valleys between roughness elements seems unlikely. The flow would tend to move around and over the top of the three-dimensional roughness elements, with low velocity or stagnant fluid near the base of the elements. In cases with sparse three-dimensional roughness (e.g. the coarsest sandgrain roughness cases of Flack *et al.* 2007), some separation would occur from individual elements, but much of the flow could remain attached to the surface as it moved around the sides of the elements. With the two-dimensional bars, flow around the sides of the bars is impossible since they block the entire span. Also, one might imagine that after the boundary layer is disrupted by a bar, it has a chance to at least approach reattachment between bars. Such behaviour was shown through flow visualization by Furuya, Miyata & Fujita (1976), who investigated the flow around two-dimensional rods with various streamwise spacings. In instances where the reattachment is somewhat complete, fluid with non-zero velocity could impact the full face of the subsequent bar instead of just the top of the element. The bar would then act as a trip and produce a larger disturbance than a field of three-dimensional elements of the same height. This scenario is supported by the ratio of k_s/k , which is 3.3 for the three-dimensional mesh case, but much larger at 13.6 for the two-dimensional bars. The large-scale events shown in figure 7(b) may explain the differences in the Reynolds stress profiles observed in figures 4–6. Below, more quantitative comparisons of the flow structure are presented.

The average extent and shape of the hairpin packets can be quantified through two-point correlations of the fluctuating velocity. Figure 8(a–c) shows contours of the two-point correlations of the streamwise fluctuating velocity R_{uu} with the correlation centred at $y_{ref}/\delta = 0.4$. The three-dimensional rough- and smooth-wall results appear similar. The correlation for the two-dimensional rough case has the same shape as in the other cases, but has a noticeably larger extent in both the streamwise and wall normal directions.

The angle of inclination of R_{uu} is related to the average inclination of the hairpin packets. It was determined, as in Volino *et al.* (2007), using a least squares method to fit a line through the points farthest from the self-correlation peak on each of the five R_{uu} contour levels 0.5, 0.6, 0.7, 0.8 and 0.9 both upstream and downstream of the self-correlation peak. For the present cases, the inclination angle remains nearly constant for reference points between $y/\delta = 0.2$ and 0.5. For $y/\delta < 0.2$ the angle drops somewhat as the contours begin to merge with the wall. For $y/\delta > 0.5$ the angle decreases towards zero, as these points tend to be above the hairpin packets which produce the inclination. For $0.2 < y/\delta < 0.5$, the angles are $10.2^\circ \pm 2.7^\circ$, $11.3^\circ \pm 2.2^\circ$ and $10.6^\circ \pm 1.2^\circ$ for the smooth, three-dimensional rough and two-dimensional rough walls, respectively. The range in each case indicates the span about the average observed between $y/\delta = 0.2$ and 0.5. The difference between the cases is comparable to the scatter in the data and the range reported in the literature for smooth-wall boundary layers (e.g. Adrian, Meinhart & Tomkins 2000). Therefore the large-scale events noted in figure 7 do not significantly affect the structure angle.

The streamwise and wall normal extent of R_{uu} are shown in figures 8(d) and 8(e) as a function of the reference point. The distance Lx_{uu} is defined as in Christensen & Wu (2005) as twice the distance from the self-correlation peak to the most downstream location on the $R_{uu} = 0.5$ contour. The three-dimensional rough- and smooth-wall results agree very well, but the two-dimensional rough-wall value averages 42% larger. The wall normal extent of the R_{uu} correlation, Ly_{uu} , is determined based on the wall normal distance between the points closest and farthest from the wall on a particular contour. Figure 8(e) shows Ly_{uu}/δ as a function of y/δ using the $R_{uu} = 0.5$

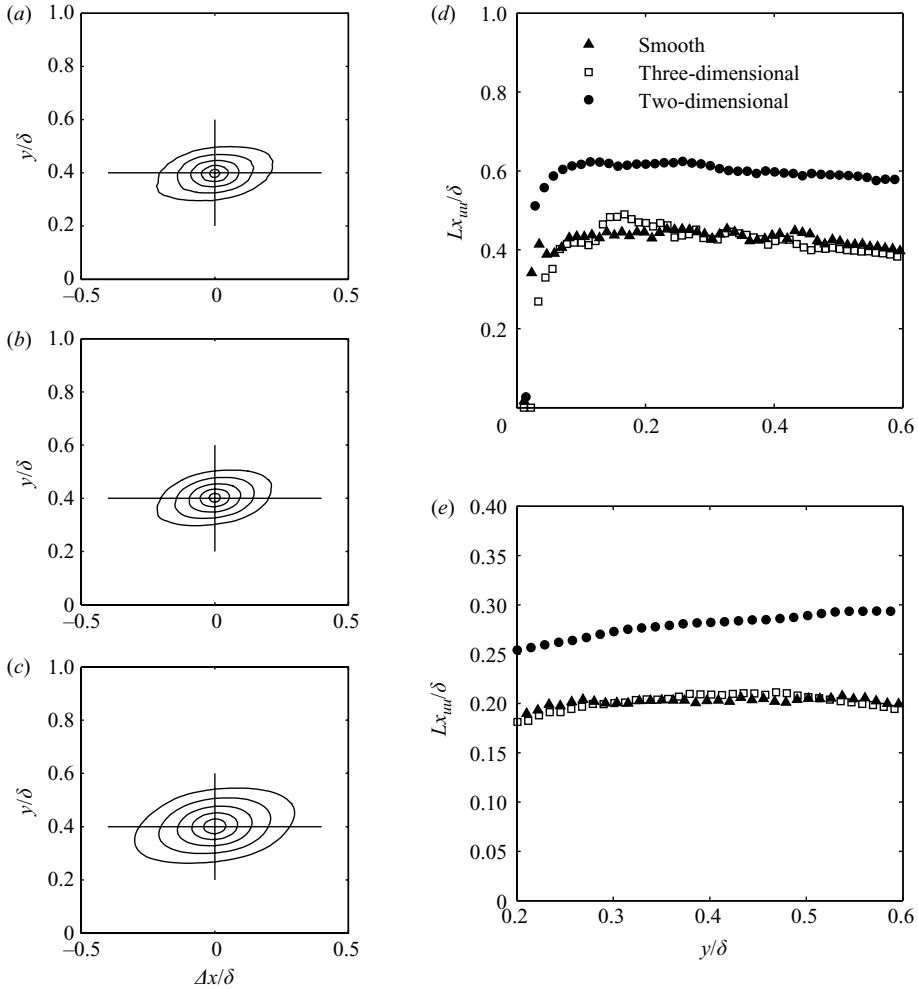


FIGURE 8. Contours of R_{uu} centred at $y/\delta = 0.4$, outermost contour $R_{uu} = 0.5$, contour spacing 0.1, (a) smooth wall, (b) three-dimensional rough wall, (c) two-dimensional rough wall, (d) streamwise extent of $R_{uu} = 0.5$ contour as function of y/δ and (e) wall normal extent of $R_{uu} = 0.5$ contour as function of y/δ .

contour. Due to the contours merging with the wall, Ly_{uu} drops towards zero for $y/\delta < 0.2$. As with Lx_{uu} , the three-dimensional rough- and smooth-wall results agree well. The Ly_{uu} value averages 39% higher for the two-dimensional rough wall case.

Figure 9 shows R_{vv} contours centred at $y/\delta = 0.4$ along with Lx_{vv} and Ly_{vv} as functions of y/δ . The length Lx_{vv} is determined based on the streamwise distance between the most upstream and downstream points on the $R_{vv} = 0.5$ contour. The length Ly_{vv} is defined as above for the R_{uu} results. The streamwise extent of R_{vv} is considerably less than that of R_{uu} , since R_{uu} is tied to the common convection velocity of each hairpin packet. The ratio Lx_{vv}/Ly_{vv} is about 0.8 for all walls. Both the streamwise and wall normal length scales are essentially equal for the smooth and three-dimensional rough walls, and average 35% and 40% larger on the two-dimensional rough wall for Lx_{vv} and Ly_{vv} , respectively. The outer layer similarity in

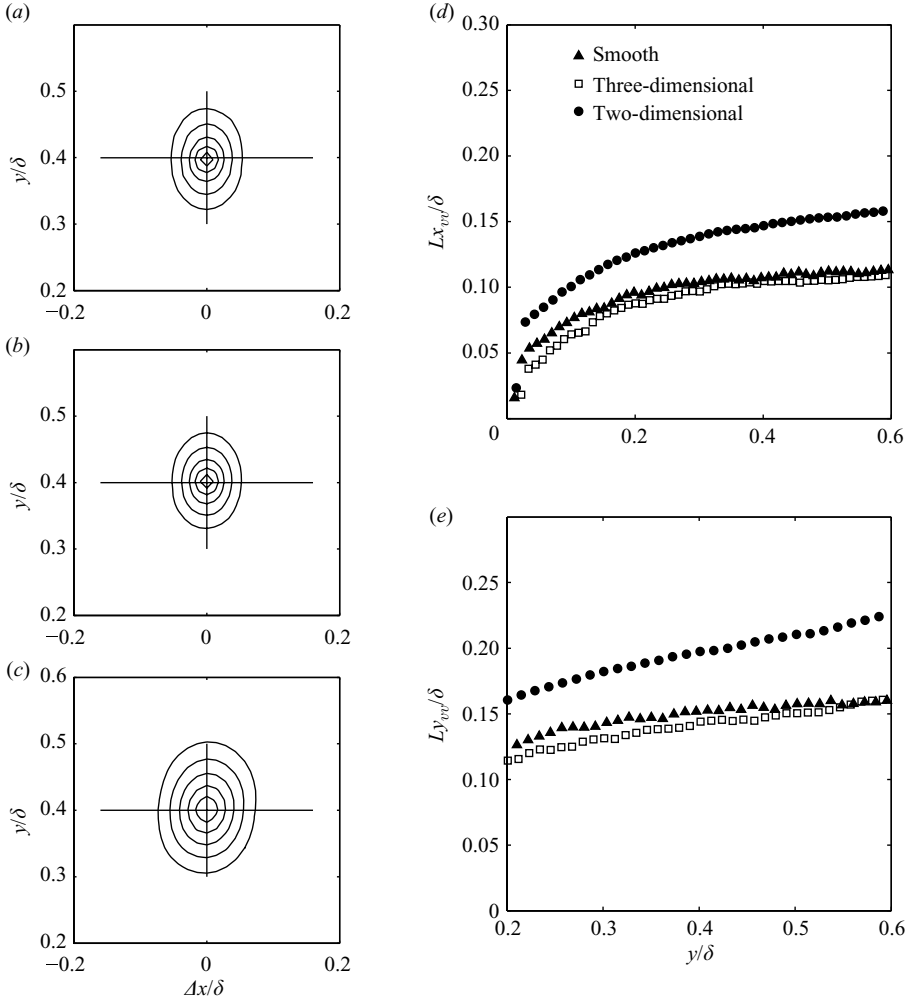


FIGURE 9. Contours of R_{vv} centred at $y/\delta = 0.4$, outermost contour $R_{vv} = 0.5$, contour spacing 0.1, (a) smooth wall, (b) three-dimensional rough wall, (c) two-dimensional rough wall, (d) streamwise extent of $R_{vv} = 0.5$ contour as function of y/δ , (e) wall normal extent of $R_{vv} = 0.5$ contour as function of y/δ .

the spatial correlations of the streamwise velocity and wall-normal velocity were also noted by Wu & Christensen (2007) for smooth and three-dimensional rough walls.

Contours of the cross-correlation R_{uv} centred at $y/\delta = 0.4$ are shown in figure 10 along with Lx_{uv} and Ly_{uv} as functions of y/δ . The lengths are computed as for R_{vv} , but are based on the -0.15 contour. As with R_{uu} and R_{vv} , the smooth- and three-dimensional rough-wall results are essentially equal. For the two-dimensional rough wall, Lx_{uv} averages 36% larger and Ly_{uv} averages 45% larger than that in the comparison cases.

Contours of the auto-correlation of the signed swirl strength $R_{\lambda\lambda}$ at $y/\delta = 0.4$ are shown in figure 11 along with $Lx_{\lambda\lambda}$ and $Ly_{\lambda\lambda}$, which are based on the $R_{\lambda\lambda} = 0.5$ contour. The three-dimensional rough- and smooth-wall results are again in very close agreement. As with the other correlations, the spatial extent is larger in the two-dimensional rough-wall case, by an average of 55% in $Lx_{\lambda\lambda}$ and 64% in $Ly_{\lambda\lambda}$.

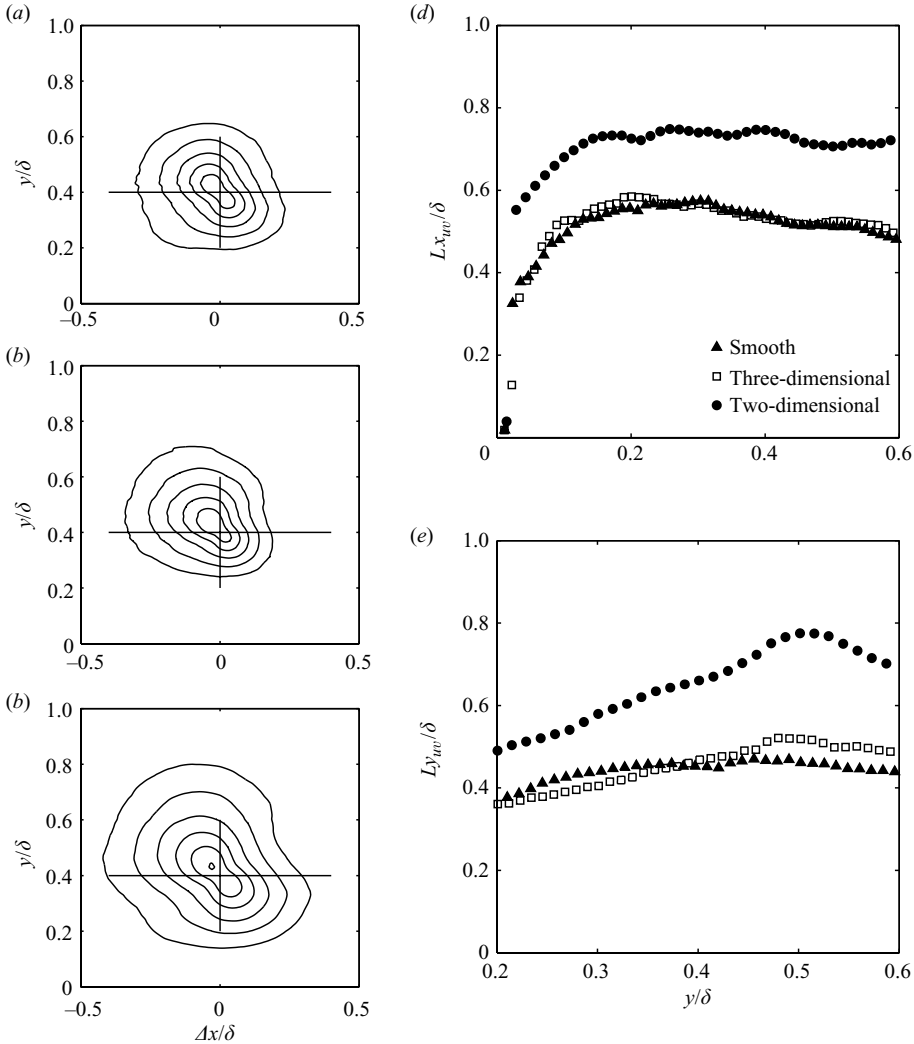


FIGURE 10. Contours of R_{uv} centred at $y/\delta=0.4$, outermost contour $R_{uv} = -0.15$, contour spacing -0.05 , (a) smooth wall, (b) three-dimensional rough wall, (c) two-dimensional rough wall, (d) streamwise extent of $R_{uv} = -0.15$ contour as function of y/δ and (e) wall normal extent of $R_{uv} = -0.15$ contour as function of y/δ .

Both $Lx_{\lambda\lambda}$ and $Ly_{\lambda\lambda}$ rise slightly with y/δ in the two-dimensional rough case, while they decrease for the other two cases. The difference is lower for the higher valued contours.

In summary, the shapes of the two-point correlations are similar for all three walls, but the spatial extent of the correlations is about 40% larger for the two-dimensional rough-wall case. This is consistent with the presence of the large-scale motions noted in figure 7(b) for the two-dimensional rough-wall case. The rise in the extent of the swirl strength correlation towards the edge of the boundary layer in this case is also consistent with the large-scale motion of fluid to the outer part of the boundary layer.

The LSE conditioned on prograde swirl events at $y/\delta = 0.4$ are shown in figure 12. Each vector in the field is normalized for presentation by its own magnitude, so

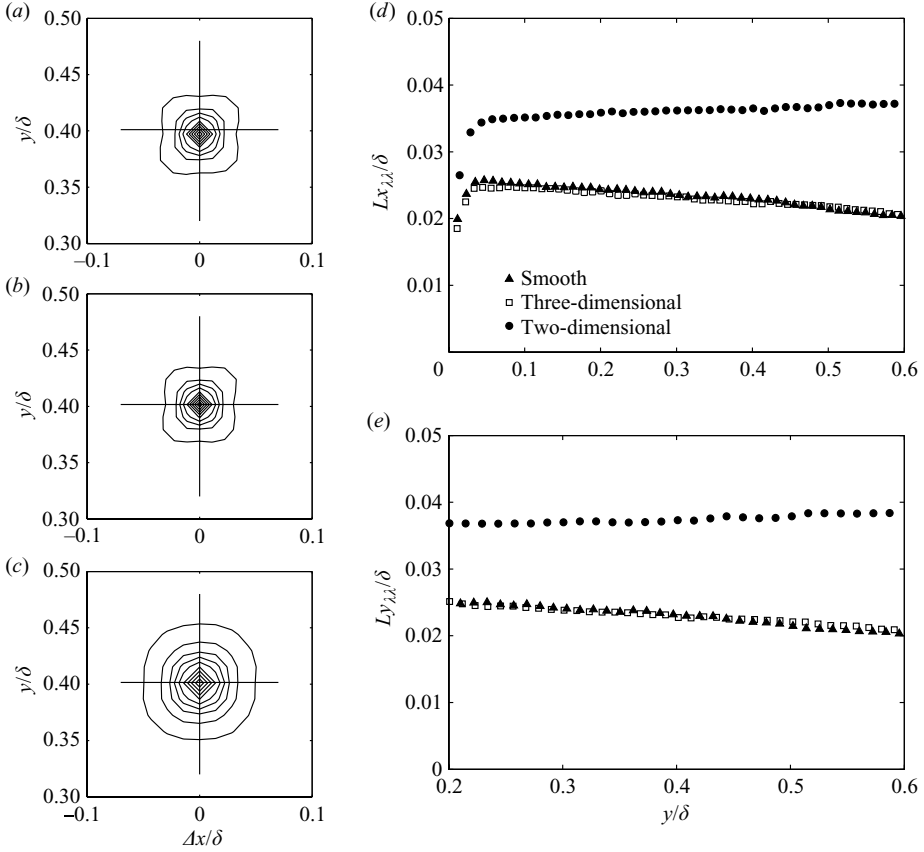


FIGURE 11. Contours of $R_{\lambda\lambda}$ centred at $y/\delta = 0.4$, outermost contour $R_{\lambda\lambda} = 0.5$, contour spacing 0.1, (a) smooth wall, (b) three-dimensional rough wall, (c) two-dimensional rough wall, (d) streamwise extent of $R_{\lambda\lambda} = 0.5$ contour as function of y/δ and (e) wall normal extent of $R_{\lambda\lambda} = 0.5$ contour as function of y/δ .

the arrows are all the same length and indicate only the average flow direction. This normalization prevents domination of the field by the vectors very close to the reference point. Qualitatively, the vector fields for all three walls are alike. As expected, the vectors show a prograde swirl at the reference location, as this was the conditioning event. There is a ‘crease’ extending both upstream and downstream of the reference point which is inclined at $13^\circ \pm 0.5^\circ$ to the wall in all three cases. Along the crease are other prograde rotations spaced roughly 0.5 to 1δ apart in the streamwise direction, suggesting a hairpin packet. The 13° angle is in good agreement with the hairpin packet angle of Adrian *et al.* (2000), the channel flow LSE results of Christensen & Adrian (2001) and the boundary layer LSE results of Hambleton *et al.* (2006). The angle is within 3° of the R_{uu} inclination angle presented in figure 9. Surrounding the inclined crease is a region of organized motion. The vectors below the crease are pointing generally upstream and towards the crease. Those above the crease are pointing generally downstream towards the crease. Outside the organized region, the vector orientations appear random. The shape of the organized region is similar for all cases. The organized region in the three-dimensional rough- and smooth-wall cases extends about 1.5δ upstream of the reference point and about

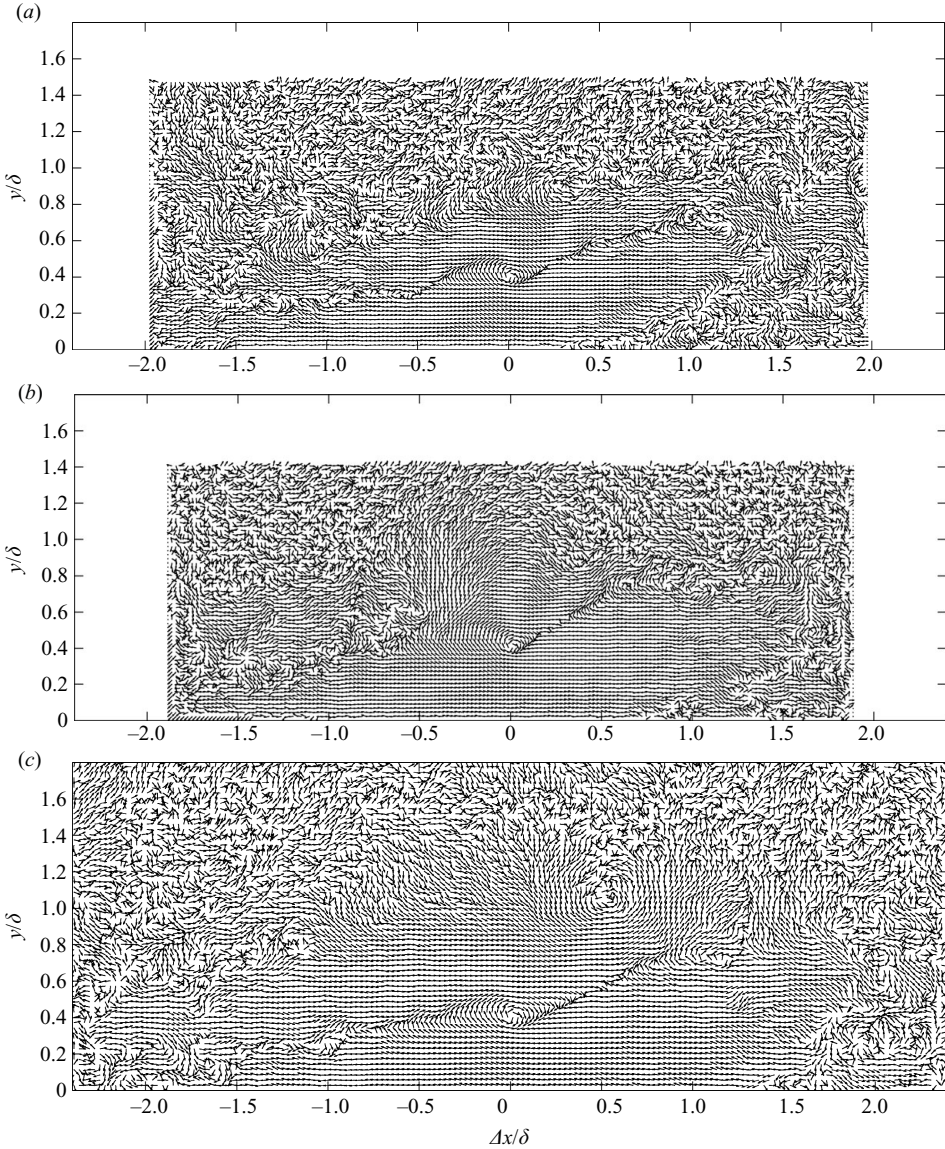


FIGURE 12. LSE conditioned on prograde swirl events at $y/\delta = 0.4$, (a) smooth wall, (b) three-dimensional rough wall and (c) two-dimensional rough wall.

1.25 δ downstream. In the vertical direction it extends from the wall to about 0.8 δ above the reference point. In the two-dimensional rough-wall case the extent of the organized region is larger, extending from about -2.25δ to 1.75δ in the horizontal direction and from the wall to about 1.1δ in the vertical direction. Matching the correlation results presented in figures 8–11, the LSE results indicate that the extent of the average hairpin packet is about 40 % larger in the two-dimensional rough case than in the other two cases.

LSE results conditioned on $u'v' < 0$ events at $y/\delta = 0.4$ are shown in figure 13. In all three cases the vectors around the reference location point away from the wall and upstream, indicating that ejections (Q2) dominate sweeps (Q4). The crease described

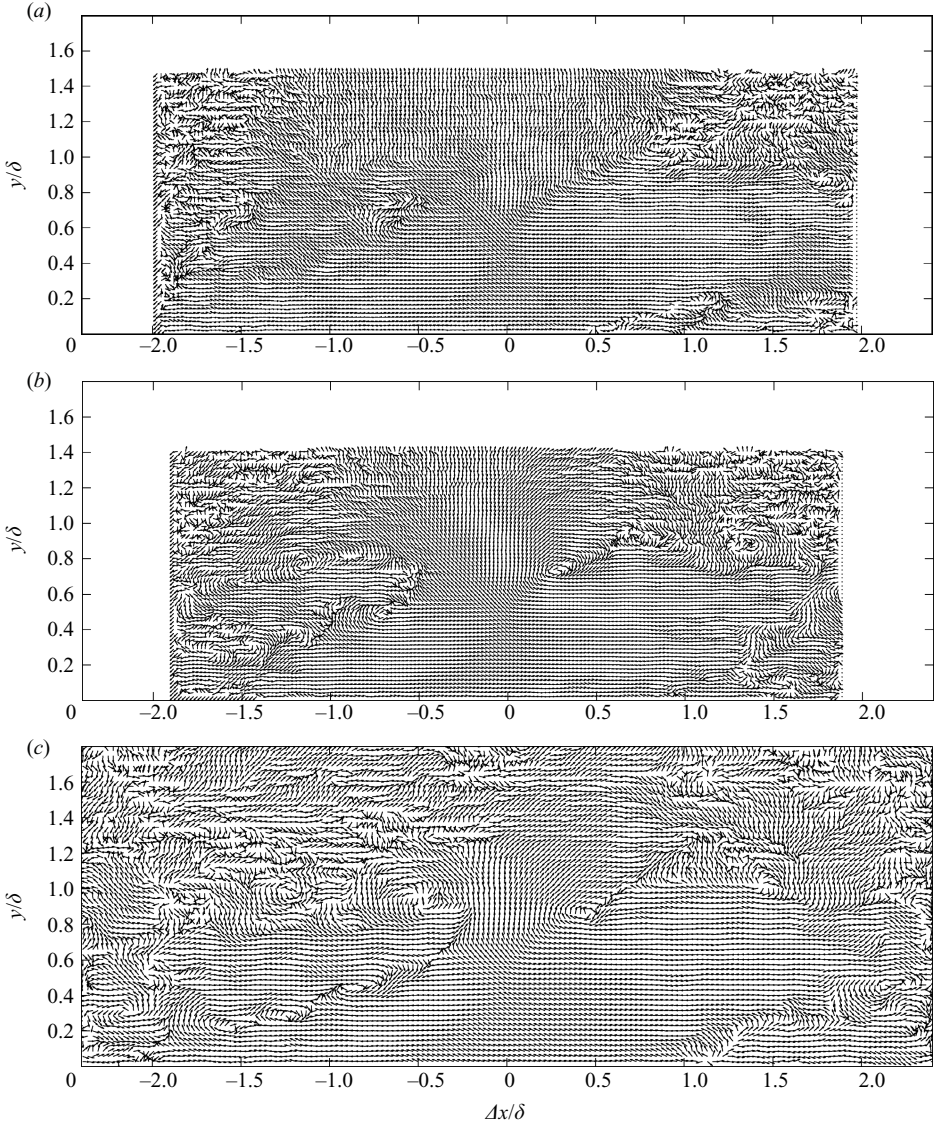


FIGURE 13. LSE conditioned on $u'v' < 0$ events at $y/\delta = 0.4$, (a) smooth wall, (b) three-dimensional rough wall and (c) two-dimensional rough wall.

in figure 12 does not cross through the reference location in figure 13, but is visible to either side. Its inclination angle varies between 14° and 17° , which is close to the angle in figure 12. This is in agreement with Marusic & Heuer (2007) who found an average angle of 14.4° based on correlations of the wall shear and the streamwise velocity which spanned three decades in Reynolds number. Prograde vortices lie along the crease, most clearly in the two-dimensional rough-wall case and least clearly in the smooth-wall case. In the two-dimensional rough-wall case, a vortex along the crease is visible as far as 1.5δ upstream of the reference location and within 0.25δ of the wall. A prograde vortex appears 0.27δ downstream and 0.32δ above the reference point in the three-dimensional rough-wall case, and a similar vortex appears 0.42δ downstream and 0.46δ above the reference point in the two-dimensional rough-wall

case. The distance from the reference point to this downstream vortex is about 45% larger in the two-dimensional rough-wall case, which is consistent with the larger scales in the case noted above. The slope of a line between the reference location and the downstream vortex is about 48° in both cases. These are hairpin vortex signatures which Adrian *et al.* (2000) noted are inclined at about 45° on a smooth wall. Above and below the crease in figure 13, the region of organized flow appears somewhat larger than that in figure 12. The organized region extends farther upstream and downstream, and farther from the wall, extending beyond 1δ above the reference point in all cases.

The correlation of the vector field to a prograde swirl event in figure 12 is expected, as hairpin packets are the dominant outer layer structure in turbulent boundary layers and hairpin heads have prograde swirl. The large spatial extent of the correlation to $u'v'$ in figure 13 is striking. It appears that vortex packets are very closely associated with Reynolds shear in the boundary layer, in agreement with the findings of Guala, Hommema & Adrian (2006) and Ganapathisubramani, Longmire & Marusic (2003). This is illustrated again in figure 14, which shows the LSE conditioned on $u'v' < 0$ with the reference location at $y/\delta = 0.7$. Even this far from the wall, the extent of the organized flow region is very large, extending past the edges of the field of view. As in figure 13, the vectors point away from the wall and upstream at the reference point indicating a dominance of ejections. The dominant feature in all three cases is a prograde vortex located above and downstream of the reference location. In the smooth-wall case it is located 0.2δ downstream and 0.25δ above the reference point. In the three-dimensional rough-wall case it is 0.17δ downstream and 0.16δ above. In the two-dimensional rough-wall case the vortex is 0.3δ downstream and 0.3δ above the reference location. The slope of a line between the reference location and the vortex in all three cases is again close to the expected 45° inclination angle for a hairpin vortex. A feature nearer the wall can be seen in the fields in figure 14 as a crease starting near the wall at $\Delta x/\delta$ between 0 and 0.5 and extending upward and downstream at about a 22° inclination. It is clearer in the rough-wall cases than in the smooth-wall case. Although no complete vortices are visible along these creases, the sense of rotation is retrograde. Similar features are visible (figure 13), starting near the wall at $\Delta x/\delta$ near 1. Possibly this near-wall crease indicates motion induced by the packet on its underside. That an event at $y/\delta = 0.7$ should be correlated to an event very near the wall suggests the importance of the outer flow structure in determining the boundary layer behaviour. It supports the findings of Wark, Naguib & Robinson (1991), Tomkins & Adrian (2005) and Hutchins & Marusic (2007), who noted that the influence of the outer layer structures extends all the way to the near-wall region.

3.3. Velocity fields: xz -plane

Instantaneous vector fields in the xz -plane were essentially the same as those shown for the three-dimensional rough- and smooth-wall cases in Volino *et al.* (2007). The fields included irregular streamwise stripes of high- and low-speed fluid with typical lengths of the order of the measurement field or larger, and typical widths were about 0.4δ . Such stripes have been described by several researchers (e.g. Hutchins & Marusic 2007). The low-speed stripes were flanked by oppositely signed swirl on either side. As described in Ganapathisubramani *et al.* (2003), Tomkins & Adrian (2003) and Volino *et al.* (2007), the vortices associated with the swirl are presumed to be the legs of hairpin or cane vortices, with the low-speed region caused by the hairpin packet above. The relationship between the low-speed regions, the hairpin legs and the hairpin

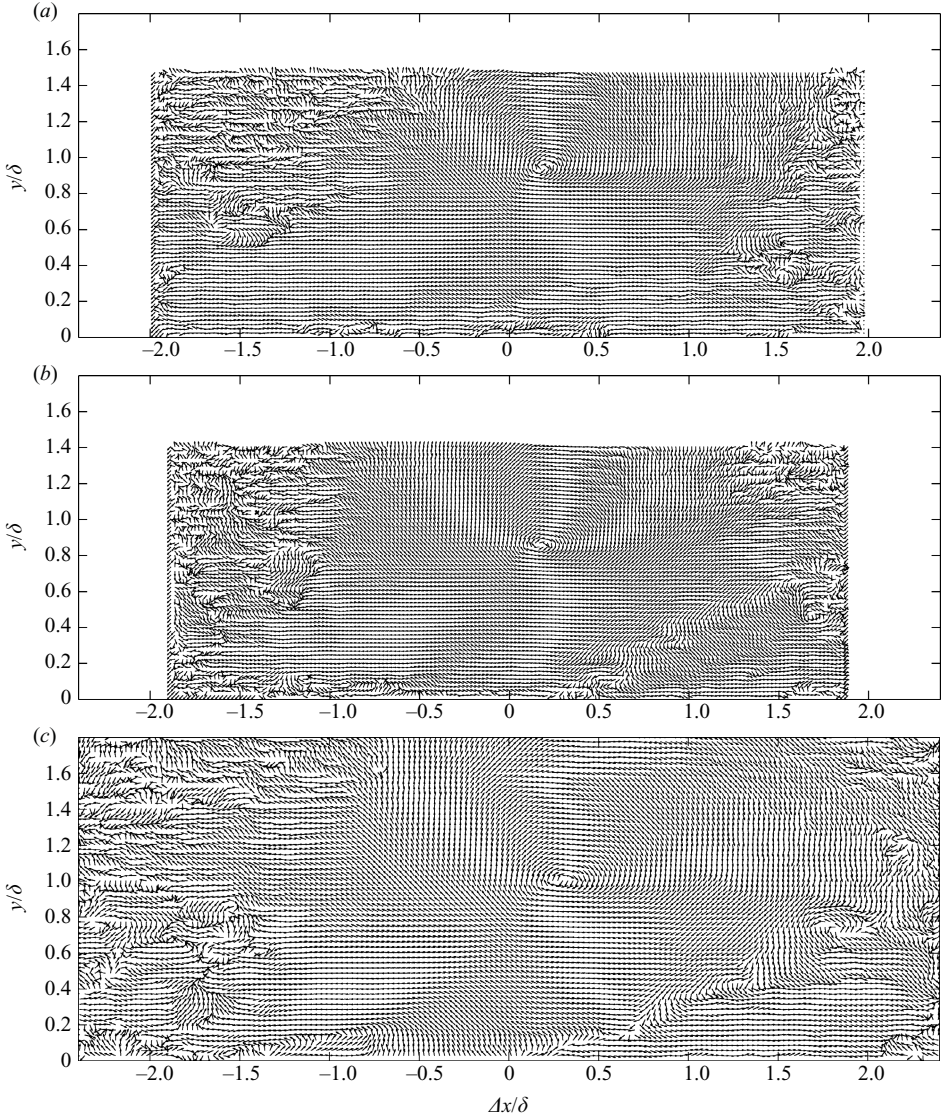


FIGURE 14. LSE conditioned on $u'v' < 0$ events at $y/\delta = 0.7$, (a) smooth wall, (b) three-dimensional rough wall and (c) two-dimensional rough wall.

heads was clearly shown by Hambleton *et al.* (2006) who acquired simultaneous measurements in streamwise-wall normal and streamwise-spanwise planes.

To quantify any differences between the smooth- and rough-wall cases, contours of the two-point correlation, R_{uu} , are shown in figure 15 for the three cases at $y/\delta = 0.1$ and 0.4. The streamwise extent of the high peak centred at the self-correlation point is about the same at $y/\delta = 0.1$ and 0.4. The streamwise extents agree with those found in the xy -plane (figure 8) to within 15%. The spanwise extent of the central peak, Lz_{uu} , is about 40% larger at $y/\delta = 0.4$ than at $y/\delta = 0.1$. The negative peaks to either side of the central peak show the correlation between adjacent high- and low-speed regions. The negative peaks also have larger spacing farther from the wall. Comparing the cases for the three different walls, Lz_{uu} agrees very closely for the

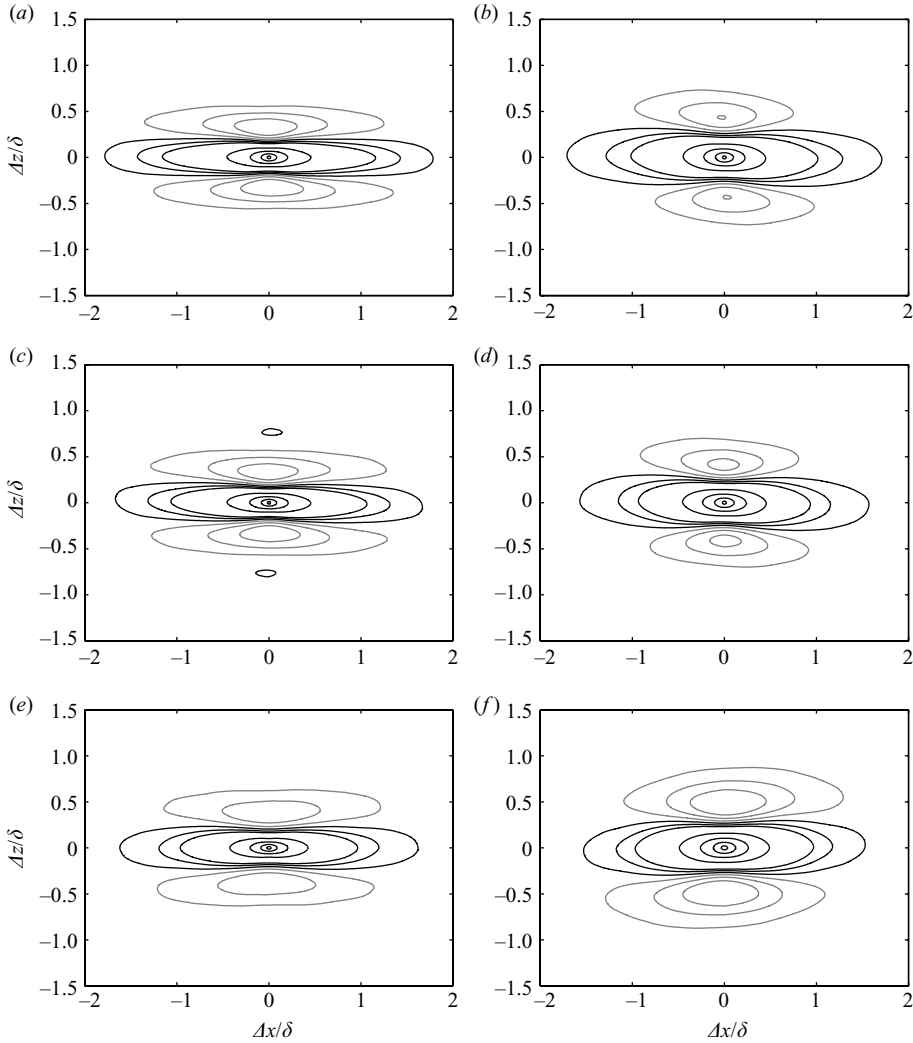


FIGURE 15. Contours of R_{uu} in xz -plane, contour magnitudes $R_{uu}=0.02, 0.06, 0.1, 0.3, 0.5, 0.7, 0.9$, contour signs black: positive, grey: negative, (a) smooth wall $y/\delta=0.1$, (b) smooth wall $y/\delta=0.4$, (c) three-dimensional rough wall $y/\delta=0.1$, (d) three-dimensional rough wall $y/\delta=0.4$, (e) two-dimensional rough wall $y/\delta=0.1$ and (f) two-dimensional rough wall $y/\delta=0.4$.

three-dimensional rough- and smooth-wall cases. It is 10%–15% larger for the two-dimensional rough-wall case. The larger extent for the two-dimensional rough-wall case agrees with the results for the xy -plane presented above, but the difference in the xz -plane is smaller. Correlations for the spanwise component of the velocity and the swirl show similar differences. The $R_{\lambda u}$ correlation is shown as an example in figure 16. The peaks to either side of the centre show the correlation of oppositely signed swirl on each side of a high- or low-speed stripe. The peaks farther from the centre show the swirl corresponding to the negative R_{uu} peaks in figure 15. As with R_{uu} , the spanwise lengths, $L_{z\lambda u}$, in figure 16 are equal for the three-dimensional rough- and smooth-wall cases, and about 15% larger for the two-dimensional rough-wall case.

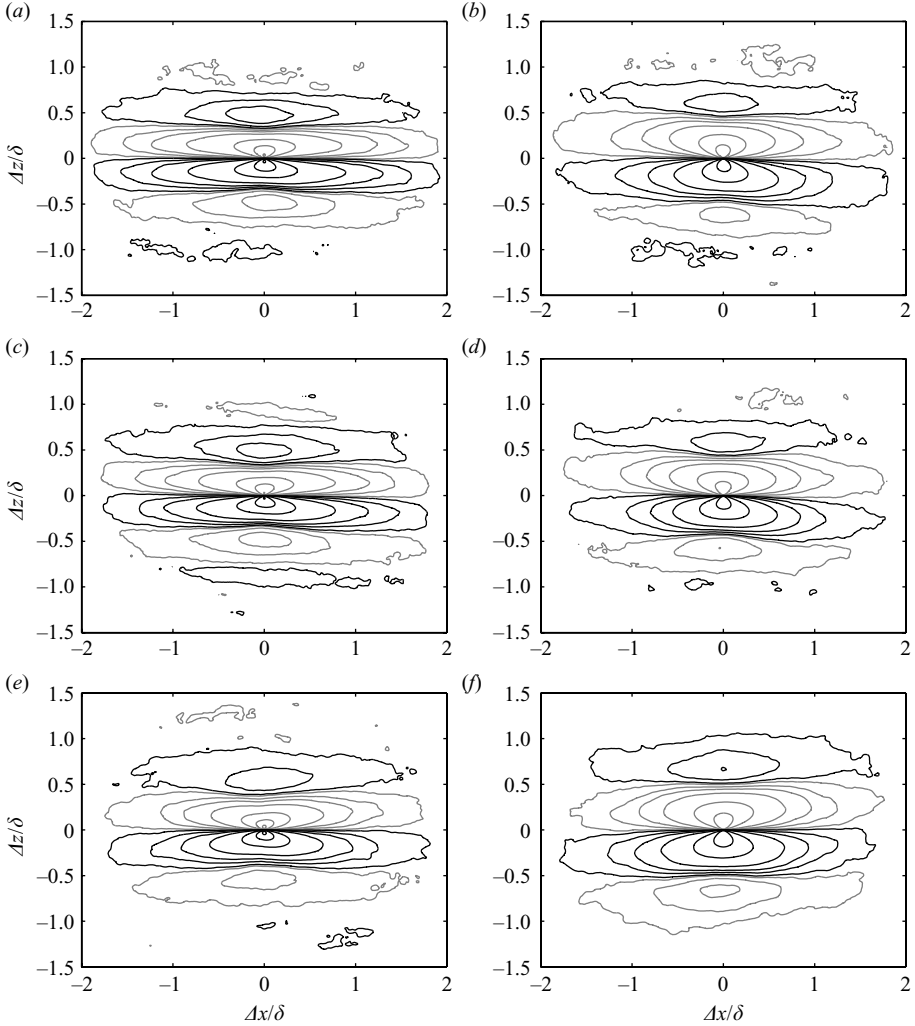


FIGURE 16. Contours of $R_{\lambda u}$ in xz -plane, contour magnitudes $R_{\lambda u} = 0.001, 0.005, 0.01, 0.02, 0.05, 0.1, 0.2$, contour signs black: positive, grey: negative, (a) smooth wall $y/\delta = 0.1$, (b) smooth wall $y/\delta = 0.4$, (c) three-dimensional rough wall $y/\delta = 0.1$, (d) three-dimensional rough wall $y/\delta = 0.4$, (e) two-dimensional rough wall $y/\delta = 0.1$ and (f) two-dimensional rough wall $y/\delta = 0.4$.

4. Discussion

Qualitatively, the correlation results indicate that although their average size may vary, the same type of hairpin packet structure is present in the outer layer in all cases. The LSE results show that shear stress in the outer layer structure correlates well with outer layer vortices. This supports the idea that the wall sets the boundary condition on which the outer flow scales, but the outer flow structure plays a large role in determining the turbulence throughout the boundary layer as pointed out by Hutchins & Marusic (2007).

The above results also show a clear difference between flows over three-dimensional and two-dimensional roughness due to the large-scale ejections into the outer boundary layer caused by two-dimensional roughness. This has been quantified

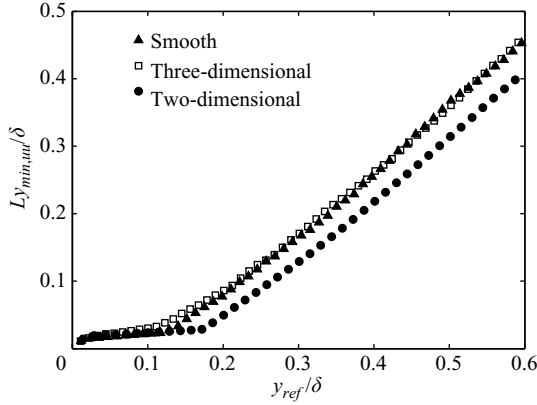


FIGURE 17. Distance from wall to closest point on $R_{uu} = 0.4$ contour, $L_{y_{min,uu}}$, as a function of the reference point for the contour.

through the large k_s/k ratio associated with the two-dimensional roughness. As discussed above and shown through flow visualization by Furuya *et al.* (1976), the flow between two-dimensional bars is able to recover and approach reattachment, resulting in a large event when it impacts the next bar. Furuya *et al.* (1976) showed that if the bars are close together, the recovery is less complete, and the disturbances created are smaller. There is an optimal p/k for creating large disturbances as frequently as possible, and as noted by Krogstad *et al.* (2005), it is near the $p/k = 8$ used in the present study. Since the large structures in the two-dimensional case are believed to originate at the bars, they indicate a direct connection of the outer flow to the wall. They would be attached eddies in the terminology of Perry & Chong (1982). In the smooth-wall and three-dimensional rough-wall cases, the outer part of the boundary layer contains only detached eddies (Perry & Marusic 1995), which have been separated from the wall. Hutchins *et al.* (2005) used a plot of $L_{y_{min,uu}}/\delta$ versus y_{ref}/δ , where $L_{y_{min,uu}}$ is the distance from the wall to the closest point on a particular R_{uu} contour and y_{ref} is the reference point for the contour, to quantify the distance that attached eddies extended into the boundary layer. For the $R_{uu} = 0.4$ contour used in figure 17, a change in the slope of $L_{y_{min,uu}}$ is clear at $y_{ref}/\delta = 0.11$ for the smooth- and three-dimensional rough-wall cases, and at $y_{ref}/\delta = 0.17$ for the two-dimensional rough-wall case. The change in slope is an indicator of the demarcation between attached and detached eddies. Its location depends on the choice of R_{uu} contour. Following the example of Hutchins *et al.* (2005), the demarcation is shown as a function of R_{uu} in figure 18. The smooth- and three-dimensional rough-wall results agree with each other and the results of Hutchins *et al.* (2005). Attached eddies extend roughly 40% farther into the boundary layer for the two-dimensional rough-wall case. If the detached eddies are similar in all turbulent boundary layers while the attached eddies depend on the wall condition, the extent of the attached eddies into the outer flow could explain the lack of similarity in the two-dimensional rough-wall case. The large-scale eddies, shown in figure 7, lead to more mixing in the outer flow and higher Reynolds stresses, as seen in figures 4–6.

The Reynolds-averaged boundary layer momentum equation

$$\rho u \frac{\partial u}{\partial x} + \rho v \frac{\partial u}{\partial y} - \frac{\partial \tau}{\partial y} + \frac{dP}{dx} = 0 \quad (4.1)$$

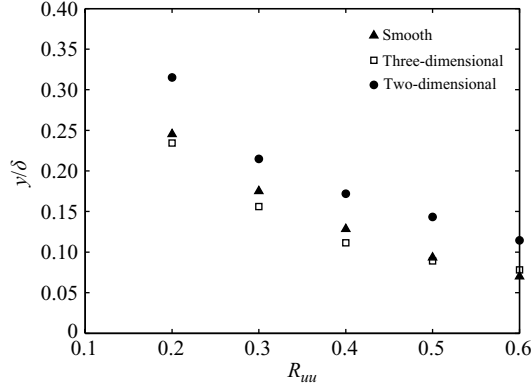


FIGURE 18. Location of slope change in $Ly_{min,uu}$ (as in figure 17) as a function of R_{uu} .

helps to explain the change in the Reynolds stresses. In a zero pressure gradient boundary layer, $dP/dx = 0$ by definition. Near the wall, in the Couette flow region, $\rho u \partial u / \partial x$ and $\rho v \partial u / \partial y$ are both small. The result is $\partial \tau / \partial y = 0$, where τ is the total shear stress. Thus τ is constant in the Couette flow region. Outside the very near-wall region, τ is essentially equal to the Reynolds shear stress. If large-scale events (attached eddies) extend farther into the boundary layer, the region of $\rho u \partial u / \partial x = \rho v \partial u / \partial y = 0$ may extend farther as well, resulting in a longer constant stress region, as seen in figure 6.

The lack of outer layer similarity in the two-dimensional rough-wall case may simply be due to the large effective roughness height relative to the boundary layer thickness. Flack *et al.* (2007) give $5k$ or $3k_s$ as a rule of thumb for the roughness sublayer thickness. For a wide range of three-dimensional roughness, k and k_s are of the same order of magnitude, so $5k$ and $3k_s$ are nearly equivalent criteria. For the present two-dimensional roughness, $k_s/k = 13.6$. In terms of $5k$, the present boundary layer is more than thick enough to expect similarity with the smooth-wall case in the outer layer. In terms of k_s , however, the entire boundary layer is within the roughness sublayer and there is no reason to expect similarity at any location. If the boundary layer was allowed to grow until δ became sufficiently larger than k_s , outer layer similarity might be observed for the two-dimensional rough-wall case. An experiment or calculation with very small two-dimensional bars, or an experiment with bars of the present size in a very long test section could provide an interesting test of this hypothesis. Another interesting test case would involve large three-dimensional roughness that is comparable in size to δ . Castro (2007) has presented mean flow results for three-dimensional rough-wall cases with very large k/δ . Roughness effects in the outer layer were not very large, but as shown in figure 3(b), the mean flow is not as strongly influenced by roughness as the Reynolds stresses (figures 4–6). Documentation of the turbulence in such cases could be helpful.

The differences observed in boundary layers over two-dimensional roughness have not been seen in channel flow. In a fully developed symmetric channel flow, the wall condition sets the wall shear, and the shear stress must go to zero at the centreline of the channel. In (4.1), the first two terms are zero when the flow is fully developed, and since dP/dx is constant, one can show that outside the very near-wall region, the $\overline{u'v'}$ profile must be linear between the limits at the wall and the centreline. This is true independent of the wall condition. Since the mean velocity profile depends on

$\overline{u'v'}$, the mean profile will also be independent of the wall condition when normalized using u_τ and the channel height. A boundary layer grows, so $\overline{u'v'}$ is not constant at a fixed distance from the wall and the $\overline{u'v'}$ profile is not linear. Instead, there is a constant stress region near the wall, which can be affected by the wall roughness, as discussed above.

Discussions presented by Adrian (2007) and Krogstad *et al.* (2005) along with the above observations are useful for considering the differences between boundary layer and channel flows in terms of turbulence structure. At the edge of a boundary layer, fluid is entrained, the boundary layer grows, and turbulent events that reach the outer part of the boundary layer can change the mean flow and Reynolds stresses there. In a channel, large-scale events generated by two-dimensional roughness may still occur, but their effect will be limited by the boundary conditions. Since the mean shear must be zero at the channel centreline, any large eddies near the centreline will be limited in their ability to produce Reynolds stresses in the mean. Also, any fluid ejected beyond the centreline of the channel will promote shear of opposite sign to the local mean shear. The result will be a cancelling of the effect of the large eddies originating on the far wall. Outer layer similarity will be maintained in spite of any large-scale events generated by the two-dimensional roughness.

5. Conclusions

An experimental study has been carried out in a turbulent boundary layer over two-dimensional roughness. Comparison with previous results indicates the present roughness leads to significant changes in the turbulence in the outer flow. An increase in the Reynolds stresses, particularly $\overline{v'^2}$ and $-\overline{u'v'}$, was observed. The mean flow was not as significantly affected. These results are consistent with the two-dimensional roughness results of Krogstad & Antonia (1999). The difference in the Reynolds stresses was due to large-scale turbulent motions emanating from the wall. These motions are associated with attached eddies, as described by Perry & Chong (1982). The large-scale attached eddies lead to an increasing spatial scale in the outer flow. The turbulence structure, however, was qualitatively similar to that observed over smooth and three-dimensional rough walls. The dominant feature of the outer flow was hairpin vortex packets having similar inclination angles in all cases. The differences observed between boundary layers over two-dimensional and three-dimensional roughness are attributable to the scales of the motion induced in each case. The largest scale motions generated by three-dimensional roughness are of the order of the roughness height k while the motions generated by two-dimensional roughness may be much larger than k due to the width of the roughness elements. This difference is exemplified by the ratio of k_s to k , where k_s is a length scale which indicates the effect of the roughness on the mean flow. For most three-dimensional roughness, k and k_s are of the same order, while for the present two-dimensional roughness $k_s/k = 13.6$. It would also appear that there are fundamental differences in the response of internal and external flows to strong wall perturbations. Internal flows are less sensitive to roughness effects due to their boundary conditions. The boundary condition at the centreline of an internal flow fixes the shape of the turbulent shear stress profile and through the shear stress fixes the shape of the mean velocity profile. This occurs independently of the wall boundary condition. In an external flow, there is no similar constraint on the outer boundary, so wall effects can have a larger influence in the outer flow.

The authors would like to thank the Office of Naval Research for providing financial support under Grants N00014-08-WR-2-0081 and N00014-08-WR-2-0159, the United States Naval Academy Hydromechanics Laboratory for providing technical support and Professor H. J. Sung for providing DNS results for comparisons.

REFERENCES

- ADRIAN, R. J. 1983 Laser velocimetry. In *Fluid Mechanics Measurements* (ed. R. J. Goldstein). Hemisphere Publishing.
- ADRIAN, R. J. 2007 Hairpin vortex organization in wall turbulence. *Phys. Fluids* **19**, Article no. 041301
- ADRIAN, R. J., MEINHART, C. D. & TOMKINS, C. D. 2000 Vortex organization in the outer region of the turbulent boundary layer. *J. Fluid Mech.* **422**, 1–54.
- ADRIAN, R. J. & MOIN, P. 1988 Stochastic estimation of organized turbulent structure – homogeneous shear-flow. *J. Fluid Mech.* **190**, 531–559.
- BURATTINI, P., LEONARDI, S., ORLANDI, P. & ANTONIA, R. A. 2008 Comparison between experiments and direct numerical simulations in a channel flow with roughness on one wall. *J. Fluid Mech.* **600**, 403–426.
- CASTRO, I. P. 2007 Rough-wall boundary layers: mean flow universality. *J. Fluid Mech.* **585**, 469–485.
- CHENG, H. & CASTRO, I. P. 2002 Near wall flow over urban like-roughness. *Boundary-Layer Met.* **104**, 229–259.
- CHONG, M. S., PERRY, A. E. & CANTWELL, B. J. 1990 A general classification of 3-dimensional flow-fields. *Phys. Fluids A-Fluid Dyn.* **2**, 765–777.
- CHRISTENSEN, K. T. & ADRIAN, R. J. 2001 Statistical evidence of hairpin vortex packets in wall turbulence. *J. Fluid Mech.* **431**, 433–443.
- CHRISTENSEN, K. T. & WU, Y. 2005 Characteristics of vortex organization in the outer layer of wall turbulence. In *Proceedings of Fourth International Symposium on Turbulence and Shear Flow Phenomena*, Williamsburg, Virginia, vol. 3, pp. 1025–1030.
- DJENIDI, L., ANTONIA, R. A., AMIELH, M. & ANSELMET, F. 2008 A turbulent boundary layer over a two-dimensional rough wall. *Exps. Fluids* **44**, 37–47.
- FLACK, K. A., SCHULTZ, M. P. & CONNELLY, J. S. 2007 Examination of a critical roughness height for boundary layer similarity. *Phys. Fluids* **19**, Article no. 095104.
- FLACK, K. A., SCHULTZ, M. P. & SHAPIRO, T. A. 2005 Experimental support for Townsend’s Reynolds number similarity hypothesis on rough walls. *Phys. Fluids* **17**, Article no. 035102.
- FLORES, O. & JIMÉNEZ, J. 2006 Effect of wall-boundary disturbances on turbulent channel flows. *J. Fluid Mech.* **566**, 357–376.
- FURUYA, Y., MIYATA, M. & FUJITA, H. 1976 Turbulent boundary layer and flow resistance on plates roughened by wires. *J. Fluids Engng* **98**, 635–644.
- GANAPATHISUBRAMANI, B., HUTCHINS, N., LONGMIRE, E. K. & MARUSIC, I. 2005 Investigation of large-scale coherence in a turbulent boundary layer using two-point correlations. *J. Fluid Mech.* **524**, 57–80.
- GANAPATHISUBRAMANI, B., LONGMIRE, E. K. & MARUSIC, I. 2003 Characteristics of vortex packets in turbulent boundary layers. *J. Fluid Mech.* **478**, 35–46.
- GUALA, M., HOMMEMA, S. E. & ADRIAN, R. J. 2006 Large-scale and very-large-scale motions in turbulent pipe flow. *J. Fluid Mech.* **554**, 521–542.
- HAMBLETON, W. T., HUTCHINS, N. & MARUSIC, I. 2006 Simultaneous orthogonal-plane particle image velocimetry measurements in a turbulent boundary layer. *J. Fluid Mech.* **560**, 53–64.
- HUTCHINS, N., HAMBLETON, W. T. & MARUSIC, I. 2005 Inclined cross-stream stereo particle image velocimetry measurements in turbulent boundary layers. *J. Fluid Mech.* **541**, 21–54.
- HUTCHINS, N. & MARUSIC, I. 2007 Evidence of very long meandering features in the logarithmic region of turbulent boundary layers. *J. Fluid Mech.* **579**, 1–28.
- IKEDA, T. & DURBIN, P. A. 2007 Direct simulations of a rough-wall channel flow. *J. Fluid Mech.* **571**, 235–263.
- JIMÉNEZ, J. 2004 Turbulent flows over rough walls. *Annu. Rev. Fluid Mech.* **36**, 173–196.
- KEIRSBULCK, L., LABRAGA, L., MAZOUZ, A. & TOURNIER, C. 2002 Surface roughness effects on turbulent boundary layer structures. *J. Fluids Engng* **124**, 127–135.

- KLINE, S. J., REYNOLDS, W. C., SCHRAUB, F. A. & RUNSTADLER, P. W. 1967 The structure of turbulent boundary layers. *J. Fluid Mech.* **30**, 741–773.
- KROGSTAD, P.-Å. & ANTONIA, R. A. 1999 Surface roughness effects in turbulent boundary layers. *Exps. Fluids* **27**, 450–460.
- KROGSTAD, P.-Å., ANDERSSON, H. I., BAKKEN, O. M. & ASHRAFIAN, A. 2005 An experimental and numerical study of channel flow with rough walls. *J. Fluid Mech.* **530**, 327–352.
- KUNKEL, G. J. & MARUSIC, I. 2006 Study of the near-wall-turbulent region of the high-Reynolds-number boundary layer using an atmospheric flow. *J. Fluid Mech.* **548**, 375–402.
- LEE, S. H. & SUNG, H. J. 2007 Direct numerical simulation of the turbulent boundary layer over a rod-roughened wall. *J. Fluid Mech.* **584**, 125–146.
- MARUSIC, I. & HEUER, W. D. C. 2007 Reynolds number Invariance of the structure inclination angle in wall turbulence. *Phys. Rev. Lett.* **99**, Article no. 114504.
- PERRY, A. E. & CHONG, M. S. 1982 On the mechanism of wall turbulence. *J. Fluid Mech.* **119**, 173–217.
- PERRY, A. E. & MARUSIC, I. 1995 A wall-wake model for the turbulence structure of boundary layers. Part 1. Extension of the attached eddy hypothesis. *J. Fluid Mech.* **298**, 361–388.
- PERRY, A. E., SCHOFIELD, W. H. & JOUBERT, P. 1969 Rough wall turbulent boundary layer. *J. Fluid Mech.* **165**, 163–199.
- SCHLICHTING, H. 1979 *Boundary-Layer Theory*, 7th ed. McGraw-Hill.
- SCHULTZ, M. P. & FLACK, K. A. 2007 The rough-wall turbulent boundary layer from the hydraulically smooth to the fully rough regime. *J. Fluid Mech.* **580**, 381–405.
- TOMKINS, C. D. & ADRIAN, R. J. 2003 Spanwise structure and scale growth in turbulent boundary layers. *J. Fluid Mech.* **490**, 37–74.
- TOMKINS, C. D. & ADRIAN, R. J. 2005 Energetic spanwise modes in the logarithmic layer of a turbulent boundary layer. *J. Fluid Mech.* **545**, 141–162.
- TOWNSEND, A. A. 1976 *The Structure of Turbulent Shear Flow*, 2nd ed. Cambridge University Press.
- VOLINO, R. J., SCHULTZ, M. P. & FLACK, K. A. 2007 Turbulence structure in rough- and smooth-wall boundary layers. *J. Fluid Mech.* **592**, 263–293.
- WARK, C. E., NAGUIB, A. M. & ROBINSON, S. K. 1991 Scaling of spanwise length scales in a turbulent boundary layer. *AIAA Paper*. 91-0235.
- WU, Y. & CHRISTENSEN, K. T. 2006 Population trends of spanwise vortices in wall turbulence. *J. Fluid Mech.* **568**, 55–76.
- WU, Y. & CHRISTENSEN, K. T. 2007 Outer-layer similarity in the presence of a practical rough-wall topography. *Phys. Fluids* **19**, Article no. 085108.
- ZHOU, J., ADRIAN, R. J., BALACHANDAR, S. & KENDALL, T. M. 1999 Mechanisms for generating coherent packets of hairpin vortices in channel flow. *J. Fluid Mech.* **387**, 353–396.